ARTICLE OPEN

Check for updates

RUNX1A isoform is overexpressed in acute myeloid leukemia and is associated with *FLT3* internal tandem duplications

Cosimo Cumbo[1,7], Francesco Tarantini[1,7], Elisa Parciante[1,7], Luisa Anelli[1], Antonella Zagaria[1], Giuseppina Biondi[2], Mariano Francesco Caratozzolo[3], Paola Orsini[4], Nicoletta Coccaro[1], Giuseppina Tota[1], Immacolata Redavid[1], Maria Rosa Conserva[1], Angela Minervini[1], Crescenzio Francesco Minervini[1], Vito Pier Gagliardi[1], Mario Delia[1], Flaviana Marzano[3], Claudia Telegrafo[3], Sharon Natasha Cox[5], Annalisa Natalicchio[2], Bachir Balech[3], Apollonia Tullo[3], Mattia Gentile[4], Francesco Giorgino[2], Giorgina Specchia[6], Pellegrino Musto[1] and Francesco Albano[1]✉

RUNX1A is the shortest and least expressed of the *RUNX1* three main isoforms (A, B, C); despite this, the leukemogenic role of its overexpression has been clearly described. Several studies have shown *RUNX1A* involvement in different blood cancers and pilot observations in acute leukemia have been reported. In this context, we evaluated *RUNX1* isoforms expression in a cohort of acute myeloid leukemia (AML) patients, finding overexpression of *RUNX1A* and *RUNX1B*, with higher median levels in thrombocytopenic cases. No difference was observed for *RUNX1C*. *RUNX1A* overexpression is higher in more immature AML phenotypes. According to the mutational profile, *FLT3* internal tandem duplication (ITD) positive cases have the highest *RUNX1A* levels and the presence of *FLT3*-ITD was the only molecular variable able to influence *RUNX1A* expression. *RUNX1A* overexpression is disease-related, associated with a specific transcriptional profile, and reappears at relapse, with no clear kinetics except in *FLT3*-ITD cases. Overall, we demonstrate *RUNX1A* overexpression in AML and its association with the *FLT3*-ITD molecular subtype. Our data shed light on the dark side of *RUNX1* deregulation, paving the way for further investigations.

Cancer Gene Therapy (2025) 32:963–972; https://doi.org/10.1038/s41417-025-00939-z

INTRODUCTION

RUNX1 is a transcription factor that plays the role of a "master regulator of hematopoiesis" through the antagonistic action of its three major protein isoforms, named RUNX1A, B, and C [1]. In adult hematopoiesis, RUNX1B/C (453 and 480 amino acids respectively, lacking exon 7a and including exons 7b and 8) are the predominantly expressed isoforms. They are transcribed from two alternative promoters and differ by 27 amino acids at their N-terminus. RUNX1A (250 amino acids, including exon 7a, which has a stop codon) accounts for only a minor fraction of the isoform pool. It is a C-terminally truncated isoform generated by alternative splicing (Fig. 1A) [1]. RUNX1A shows enhanced DNA binding [2], specific cofactors [3] and divergent effects on target gene transcription [4] as compared to RUNX1B/C.

RUNX1A enhances self-renewal activity and hematopoietic stem cell (HSC) expansion ex vivo and in vivo [4]; furthermore, it suppresses myeloid differentiation [2]. In contrast, RUNX1B/C overexpression induces HSCs quiescence [5] and promotes differentiation [2] in murine models. For these reasons, *RUNX1A* overexpression can be leukemogenic, as suggested by pilot observations in acute leukemia [2, 6], and additional studies have shown the pathogenicity of *RUNX1A* in other blood diseases [3, 7–9].

Given the pivotal role of the *RUNX1* gene in acute myeloid leukemia (AML), we evaluated the expression of its isoforms in our series, aiming to elucidate the role of *RUNX1A* in the AML pathogenesis, its possible associations with different disease subtypes, and its influence during the disease course.

MATERIALS AND METHODS

Patients

A total of 138 consecutive newly diagnosed AML patients, diagnosed and treated at the Hematology Section of the University of Bari from 2014 to 2023, were included in this study. The main patients clinical data are summarized in Supplementary Table 1 and a more detailed patients' database is reported in Supplementary Table 2. Among them, the time of relapse of 21 cases was included in. Of the patients who underwent molecular disease monitoring (see paragraph 2.6), 11 were in complete remission (CR) and were considered. In total, 170 bone marrow (BM) samples collected and stored at the aforementioned institution were included in the study. The group of healthy controls (HC) consists of 11 samples: ten HC donors from the same institution and a commercial

[1]Department of Precision and Regenerative Medicine and Ionian Area (DiMePRe-J) - Hematology and Stem Cell Transplantation Unit - University of Bari "Aldo Moro", Bari, Italy. [2]Department of Precision and Regenerative Medicine and Ionian Area (DiMePRe-J), Section of Internal Medicine, Endocrinology, Andrology and Metabolic Diseases, University of Bari "Aldo Moro", Bari, Italy. [3]Institute of Biomembranes, Bioenergetics and Molecular Biotechnologies (IBIOM) - National Research Council (CNR), Bari, Italy. [4]Department of Human Reproductive Medicine, Medical Genetics Unit, ASL Bari, Bari, Italy. [5]Department of Biosciences, Biotechnology and Environment, University of Bari "Aldo Moro", Bari, Italy. [6]School of Medicine, University of Bari "Aldo Moro", Bari, Italy. [7]These authors contributed equally: Cosimo Cumbo, Francesco Tarantini, Elisa Parciante.
✉email: francesco.albano@uniba.it

Received: 24 April 2025 Revised: 24 June 2025 Accepted: 1 July 2025
Published online: 15 July 2025

pool of 56 HC samples (Human Bone Marrow Total RNA-Clontech Laboratories, Inc., Mountainview, CA, USA).

RUNX1 isoforms absolute quantification

Mononuclear cells were isolated from BM samples by Ficoll separation, and total RNA was extracted using the RNeasy Mini Kit (Qiagen, Hilden, Germany); the RNA concentration and purity were checked using the Qubit 2.0 fluorometer and NanoDrop UV-Vis spectrometer (Thermo Fisher Scientific, Waltham, MA). One µg of total RNA was reverse transcribed into complementary DNA (cDNA) using the QuantiTect reverse transcription kit (Qiagen).

RUNX1A/B/C isoforms were quantified by three assays according to the droplet digital PCR (ddPCR) Gene Expression EvaGreen Assays Protocol (BioRad, Hercules, CA). For *RUNX1A* (NM_001122607) and *RUNX1C* (NM_001754) two distinct pairs of specific primers were used (RUNX1A_F: A ACCCTCGTGCCTCCCTGAA and RUNX1A_R: AGCTCTATCCTGGCTGGGGA; RUNX1C_F: GGCTTCAGACAGCATATTTGAG and RUNX1C_R: AACGCCTCGCTCA TCTTG). For the *RUNX1B* transcript isoform (NM_001001890), a primer pair quantifying *RUNX1A + B* was used (RUNX1A + B_F: CCGTCTGGTAGGAGC TGTTT and RUNX1B_R: AACGCCTCGCTCATCTTG) because no unique exon-usage exists unlike for the other isoforms. Therefore, to perform the absolute quantification of *RUNX1B*, the *RUNX1A* quantification was subtracted from the *RUNX1A + B* quantification. All assays were performed as already reported [10, 11]. The target quantification was calculated as the ratio between each *RUNX1* isoform and the number of copies of *GUSB* (R/G); *RUNX1* gene expression (RUNX1all) was calculated as the sum of its three isoforms.

RUNX1A protein quantification

Mononuclear cells isolated from BM samples by Ficoll separation or purchased from StemCell™ Technologies (Cologne, Germany) were mechanically lysed using the homogenizer T10 basic Ultra-Turrax1 (IKA, Staufen, Germany) in RIPA buffer (Thermo Fisher Scientific), supplemented with cOmplete™ Protease Inhibitor Cocktail and PhosSTOP™ phosphatase inhibitor (Roche, Basel, Switzerland) to extract total proteins. The lysates were centrifuged at 13,000 × *g* at 4 °C for 10 min to remove debris, and total protein levels were quantified using the BioRad Protein Assay. Equal amounts of protein were mixed with Laemmli sample buffer, resolved by SDS-PAGE, and blotted on nitrocellulose membranes using a Trans-Blot Turbo Transfer System (BioRad). Membranes were blocked with the EveryBlot Blocking Buffer (BioRad), incubated with primary antibodies (anti-RUNX1 antibody ab240639, Abcam, MA, USA; anti-beta-actin antibody C4, sc-47778, Santa Cruz Biotechnology, Inc., TX, USA; 1:1000 dilution) overnight at 4 °C, and washed with 1X TBS-Tween 0.1%. After incubation with a horseradish-peroxidase-conjugated secondary antibody (1:3000 dilution, BioRad) for 1 h at room temperature, Clarity Western ECL Substrate (BioRad) was used for protein visualization with a ChemiDoc Imaging System (Bio-Rad). The signal intensity of the protein bands was measured using Image Lab Software (BioRad). The target quantification was calculated as the ratio between RUNX1A and beta-actin (R/B). AML samples were compared with those from HC donors and with commercial human bone marrow mononuclear cells (BMMCs) StemCell™ Technologies (Cologne, Germany).

Targeted next-generation sequencing (NGS)

NGS analysis was performed on genomic DNA extracted from BM samples at diagnosis using an AmpliSeq customized panel (Thermo Fisher Scientific) encompassing the full coding regions or specific exons of 26 target genes involved in the pathogenesis of myeloid malignancies (*ANKRD26, ASXL1, CALR, CBL, CEBPA, DDX41, DNMT3A, ETV6, EZH2, FLT3, GATA2, IDH1, IDH2, JAK2, KIT, KRAS, MPL, NPM1, NRAS, RUNX1, SF3B1, SRSF2, TET2, TP53, U2AF1, ZRSR2*), as previously reported [12–14]. Torrent Suite Software (Thermo Fisher) was used for quality control, alignment to the human genome (hg19), and variant calling, using the somatic workflow for single samples and the default parameters. Variants were annotated with Ion Reporter Software (Thermo Fisher). Variants located in intronic regions, synonymous or those present with >1% global minor allele frequency in the normal population were filtered out. Selected variants were investigated for a potential pathogenic role using the SIFT and PolyPhen scores and the Catalogue of Somatic Mutations in Cancer database [13].

FLT3 mutational analysis

FLT3 internal tandem duplication (ITD) and D835/I836 variants were investigated on BM samples at disease onset and relapse, as reported [15]. The *FLT3* ITD burden was reported as an allelic ratio (AR). Cases carrying an AR < 0.5 were defined as ITD-low, and patients with an AR ≥ 0.5 as ITD-high, according to the 2017 ELN recommendations [16]. ITD cases were also distinguished between single ITD (single duplication) and multiple ITD (≥2 different duplications), as reported [17]. According to the duplication length, patients were divided into ITD short and ITD long, using as cut-off value the median ITD length observed in our cohort (50 bps), as previously suggested [18]. Other tyrosine kinase domain (TKD) variants were identified by NGS analysis (see paragraph 2.4.).

Molecular monitoring of measurable residual disease

For AML cases carrying one of the following molecular markers: *NPM1*, *PML::RARA*, *RUNX1::RUNX1T1*, *CBFB::MYH11*, molecular monitoring was performed by RQ-PCR using the following kits (Ipsogen): NPM1 mutA MutaQuant Kit, PML-RARA bcr1/bcr3 Kit, RUNX1-RUNX1T1 Kit, CBFB-MYH11 A Kit.

Gene expression profiling

Gene expression profiling was performed by RNA-Seq. Twelve patients were sequenced using the massive sequencing Illumina NovaSeq6000 platform: seven cases with "high" *RUNX1A* expression [fold change (FC) ≥ 5] and five cases expressing "normal/low" levels (FC ≤ 3). In brief, paired-end reads obtained in FASTQ format were quality-checked using FastQC version 0.12.1. and the analysis results were summarized in a single HTML report using MultiQC [19]. Reads were trimmed using the Trimmomatic tool version 0.32 [20] to remove sequences and adapters and then mapped against the Homo sapiens reference genome (GRCh.38: https://ftp.ensembl.org/pub/release-109/fasta/homo_sapiens/dna/) using the STAR aligner [21].

Reads mapped to each gene were summarized based on the genome annotation (version 109) from the ESEMBL database (https://ftp.ensembl.org/pub/release-109/gtf/homo_sapiens/Homo_sapiens.GRCh38.109.gtf.gz) using the FeatureCounts algorithm [22]. Principal Component Analysis (PCA) was performed using the DESeq2 R package by means of regularized log transformation (rld) of read counts to illustrate the overall distance between "high" and "normal/low" *RUNX1A* expression groups.

RUNX1A reads for each sample were calculated using the TMM (Trimmed Mean of M-values), while DESeq2 was used to detect differentially expressed genes (DEGs) [23]. DEGs were selected by filtering them for Log2FC > 1.5 and < −1.5, and adjusted (adj) *p* value < 0.05. Data were visualized on a volcano plot.

Gene names and gene ontology annotations (BP Biological Process, CC Cellular Component, MF Molecular Function) of DEGs were retrieved from the Human Genome Annotation Resource (available via the org.Hs.eg.db R package) in combination with the AnnotationHub and AnnotationDbi R packages and analyzed using the Database for Annotation, Visualization and Integrated Discovery (DAVID) v2024q2 (July 2024) [24, 25]. DEGs were analyzed in QIAGEN Ingenuity Pathways Analysis (IPA) software (QIAGEN, Hilden, Germany) to categorize differentially expressed transcripts and identify significantly regulated functional pathways. The list of DEGs was used as a query in IPA. The 'core analysis' function was run to identify canonical pathways [26].

Methylation analysis

To investigate the possible role of epigenetic regulation in *RUNX1* expression, genome-wide methylation data from the TF-1 cell line stably expressing *DNMT3A* isoform 1 were used to evaluate the methylation status of CpG sites mapped to the *RUNX1* gene according to the *DNMT3A* mutation status. Specifically, methylation data from the TF-1 cell line stably expressing *DNMT3A* wild-type (WT) or AML-associated mutant hotspots at Arg822 (R882) [specifically R882C or R882H, which induce macro-oligomer formation, alone or in combination with R676K, a macro-oligomerization-reducing mutation (GEO Datasets ID: GSE226062)] were analyzed [27]. Data analysis of the IDAT raw methylation files from the Illumina Methylation EPIC BeadChip microarrays was performed using a dedicated R Bioconductor workflow that incorporated several packages for the analysis of methylation array data (https://www.bioconductor.org/packages/devel/workflows/vignettes/methylationArrayAnalysis/inst/doc/methylationArrayAnalysis.html). The IlluminaHumanMethylationEPICanno.ilm10b4.hg19 R package was used for the annotation of Illumina EPIC methylation arrays. Unsupervised hierarchical clustering of CpG sites mapping to the *RUNX1* gene was performed to assess their correlation according to the methylation status in the aforementioned cell lines.

Statistical analysis

All statistical analyses were carried out using GraphPad Prism version 8.3.0 (GraphPad Software Inc., San Diego, CA, USA). Continuous variables were

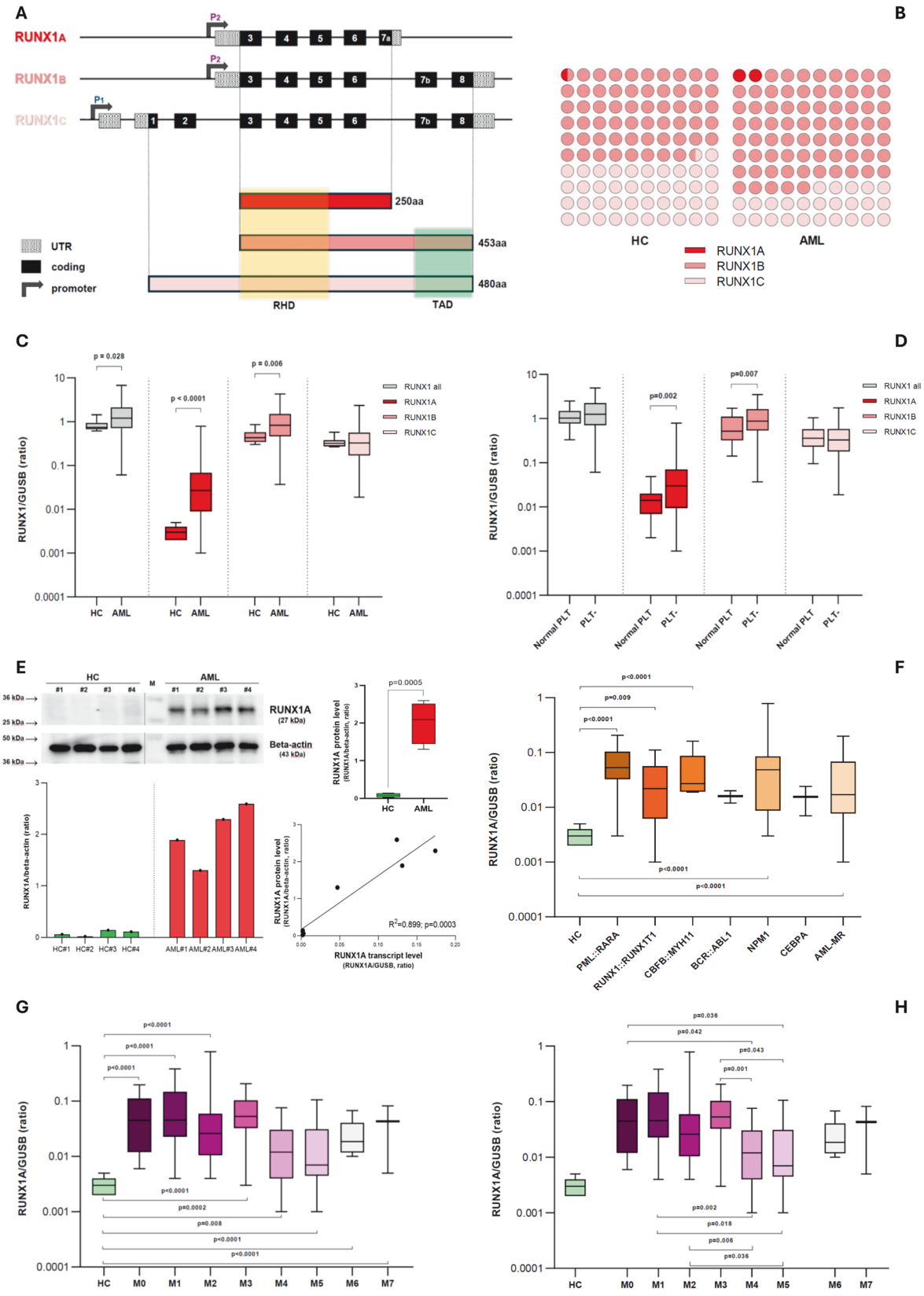

presented as median (minimum-maximum). The Shapiro-Wilk test was performed to check for the normal distribution of continuous variables. The differences in the distribution of continuous variables between categories were compared using either paired or unpiaired *t* test (for variables passing the normality test) or Mann–Whitney and Wilcoxon matched pairs tests (for variables not passing the normality test). One-way ANOVA and Kruskal-Wallis tests were used to compare the distributions of more than two groups of continuous variables. Multiple

Fig. 1 *RUNX1* isoforms molecular quantification in AML. A Schematic representation of *RUNX1* three main transcript isoforms (top) and their respective protein products (bottom). **B** *RUNX1 A*, *B*, and *C* relative quantification (as the fraction of total RUNX1 transcripts) in HC and AML samples. In the 10 × 10 dot plot the relative abundance of each isoform was reported as "part of whole"; each dot corresponds to 1% of all *RUNX1* transcripts. **C** Comparison of *RUNX1* expression between healthy controls and AML cases at diagnosis (single isoforms and their sum are reported). **D** *RUNX1* expression according to patient PLTs number. **E** Representatives immunoblot image of RUNX1A and beta-actin (top-left). As made explicit by the separating lines, the final image was obtained by splicing different sections of the same image (raw images are reported in Supplementary Fig. 2). HC#4: commercial bone marrow mononuclear cells. Densitometric analysis of RUNX1A bands expressed as relative optical density and normalized to beta-actin (bottom–left). Comparison between HC and AML RUNX1A protein levels (top–right). Simple linear regression between the *RUNX1A* transcript and protein levels (bottom-right). **F** *RUNX1A* expression according to the latest WHO AML classes. The comparisons *BCR::ABL1* vs HC and *CEBPA* vs HC were not performed, given the rarity of cases among those enrolled ($n = 2$ and $n = 2$, respectively). **G**, **H** RUNX1A transcript levels according to the FAB classes. **C-H** Boxplots representing the distribution. The boxes extend from the 25th to 75th percentiles. The line in the box represents the median value. The whiskers range from the smallest value to the largest. P1: distal promoter; P2: proximal promoter; RHD: runt-homology domain; TAD: transactivation domain; HC: healthy controls; AML: acute myeloid leukemia; PLT-: thrombocytopenic cases (<150.000 PLTs/ul); AML-MR: AML, myelodysplasia-related.

linear regression analysis was performed to test the influence of gene mutations (independent variables) on *RUNX1A* levels (dependent variable). Spearman's rank-order correlation test was conducted to determine the relationship between the RUNX1A transcript and protein levels. Simple linear regression analysis was performed to predict RUNX1A protein levels from transcript levels. Univariate and multivariate Cox regression analyses were conducted to investigate the impact of *RUNX1* isoform levels on patients' overall survival (OS). Spearman's rank-order correlation test was also performed to study the relationship between ddPCR and RNA-Seq *RUNX1A* quantifications. A p value < 0.05 was considered statistically significant.

RESULTS

RUNX1A and RUNX1B isoforms are overexpressed in newly diagnosed AML, with higher levels in thrombocytopenic cases

As observed in the normal hematopoietic system [5], among AML patients, considering median values, *RUNX1B/C* were confirmed as the dominantly expressed isoforms: 73% and 25% of the total *RUNX1* transcripts, respectively, whereas *RUNX1A* accounted for 2% of the isoforms pool (Fig. 1B). When we examined the absolute quantification of each isoform, comparing AML cases ($n = 138$) with HC ($n = 11$), we confirmed *RUNX1* overexpression in AML (1.209 vs 0.747 R/G; $p = 0.028$), as already known [28]. Moreover, we observed overexpression of *RUNX1A* (0.027 vs 0.003 R/G; $p < 0.0001$) and *RUNX1B* (0.827 vs 0.433 R/G; $p = 0.006$), whereas no difference was observed for *RUNX1C* (Fig. 1C).

Interestingly, when comparing *RUNX1* isoform expression with the patients' main clinical and biological data (Supplementary Table 1), thrombocytopenic cases ($n = 93$, <150,000 PLTs/ul) exhibited higher levels of the *RUNX1A* and *RUNX1B* isoforms compared to AMLs with normal PLTs levels ($n = 23$) (0.030 vs 0.014 R/G; $p = 0.002$ and 0.876 vs 0.517 R/G; $p = 0.007$ respectively), confirming the previously established involvement of the *RUNX1* gene in megakaryocytopoiesis (Fig. 1D) [29]. No other associations emerged from the comparisons between *RUNX1* isoforms levels and variables reported in Supplementary Table 1.

Given the known leukemogenic role of *RUNX1A* and its more pronounced overexpression compared to the other *RUNX1* isoforms (~10-fold increase between AML and HC median levels —Fig. 1C), we decided to focus on *RUNX1A* expression and its possible association with AML pathogenesis.

Firstly, we verified the RUNX1A overexpression at the protein level by immunoblot analysis (Fig. 1E). Increased RUNX1A protein levels were observed in AML patients compared to HC (2.018 vs 0.082 R/B, $p = 0.0005$), and a positive correlation was found between the RUNX1A transcript and protein levels (r_s=0.805, $p = 0.025$) (Fig. 1E). Using simple linear regression analysis to predict protein levels from transcript levels, a significant regression equation was identified [$F(1,6) = 53.55$, $p = 0.0003$] with $R^2 = 0.899$. Therefore, RUNX1A protein and transcript quantities are correlated and as expected, the former depends on the latter.

RUNX1A overexpression is independent of patient classification but related to the disease phenotype

The increased *RUNX1A* expression (in AMLs vs HC) was confirmed even when our AML cases were classified according to the latest edition of the WHO classification [30]. Considering the *RUNX1A* median value for each AML class (*PML::RARA*, $n = 12$; *RUNX1::RUNX1T1*, $n = 8$; *CBFB::MYH11*, $n = 8$; *NPM1*, $n = 22$; AML-MR, $n = 46$), the difference compared to HC remained statistically significant (Fig. 1F), whereas no changes were observed when comparing disease classes ($p = 0.371$). These observations suggested a possible *RUNX1A* involvement in AML pathogenesis independent of patient classification. The comparisons *BCR::ABL1* vs HC and *CEBPA* vs HC were not performed, given the rarity of these cases among those enrolled ($n = 2$ and $n = 2$, respectively).

Because preliminary data on acute leukemia indicated higher expression levels of *RUNX1A* in acute lymphoblastic leukemia and in AML-M2 patients [6], we classified our cases according to the older FAB classification [31], eliciting a significant difference for all morphological subtypes (M0, $n = 11$; M1, $n = 14$; M2, $n = 30$; M3, $n = 12$; M4, $n = 26$; M5, $n = 9$; M6, $n = 8$; M7, $n = 3$) compared to HC (Fig. 1G). Interestingly, the comparison between classes highlighted significant differences (Fig. 1H). In particular, the *RUNX1A* levels were higher in AML patients with a more immature phenotype and characterized by impaired granulocytic differentiation (M0-M3) as compared to cases showing a monocytic morphology (M4-M5), in line with the known *RUNX1A* ability to suppress myeloid differentiation, enhancing the self-renewal HSCs capacity [2, 4, 32]. In this context, M6 and M7 classes appeared to follow other pathways, which we cannot address given the rarity of cases among those enrolled.

FLT3-ITD mutated patients show the highest median levels of the RUNX1A isoform

Then, we subdivided our patients according to their mutational profile. Overall, *FLT3*-ITD positive cases ($n = 23$) presented the highest median *RUNX1A* levels at the disease onset (0.071 R/G), as shown in Fig. 2A. A strong relationship between the *FLT3*-ITD mutations and *RUNX1A* transcript levels was confirmed by multiple linear regression analysis. Specifically, between all gene mutations detected in our cohort (*TP53*, $n = 7$; *NPM1*, $n = 22$; *CEBPA*, $n = 2$; *RUNX1*, $n = 11$; *FLT3*-ITD, $n = 23$; *FLT3*-TKD, $n = 10$; *DNMT3A*, $n = 8$; *TET2*, $n = 17$; *IDH2*, $n = 8$; *EZH2*, $n = 3$; *ASXL1*, $n = 16$; *SRSF2*, $n = 6$; *SF3B1*, $n = 3$; *U2AF1*, $n = 5$; *ETV6*, $n = 3$; *CBL*, $n = 3$; *NRAS*, $n = 15$; *GATA2*, $n = 3$), the presence of *FLT3*-ITD was the only variable able to influence the *RUNX1A* levels ($p = 0.0005$; Supplementary Table 3). On this basis, we explored the possible connection between *FLT3* mutational status and *RUNX1A* expression (Fig. 2B). A significant difference was observed between *FLT3*-mutated ($n = 33$) and *FLT3*-wt AML ($n = 82$) (0.048 vs 0.020 R/G, $p = 0.019$), but this difference became more evident when we compared *FLT3*-ITD ($n = 23$) with *FLT3*-wt ($n = 82$) cases (0.071 vs 0.020 R/G, $p < 0.0001$). While *FLT3*-ITD AML exhibited higher

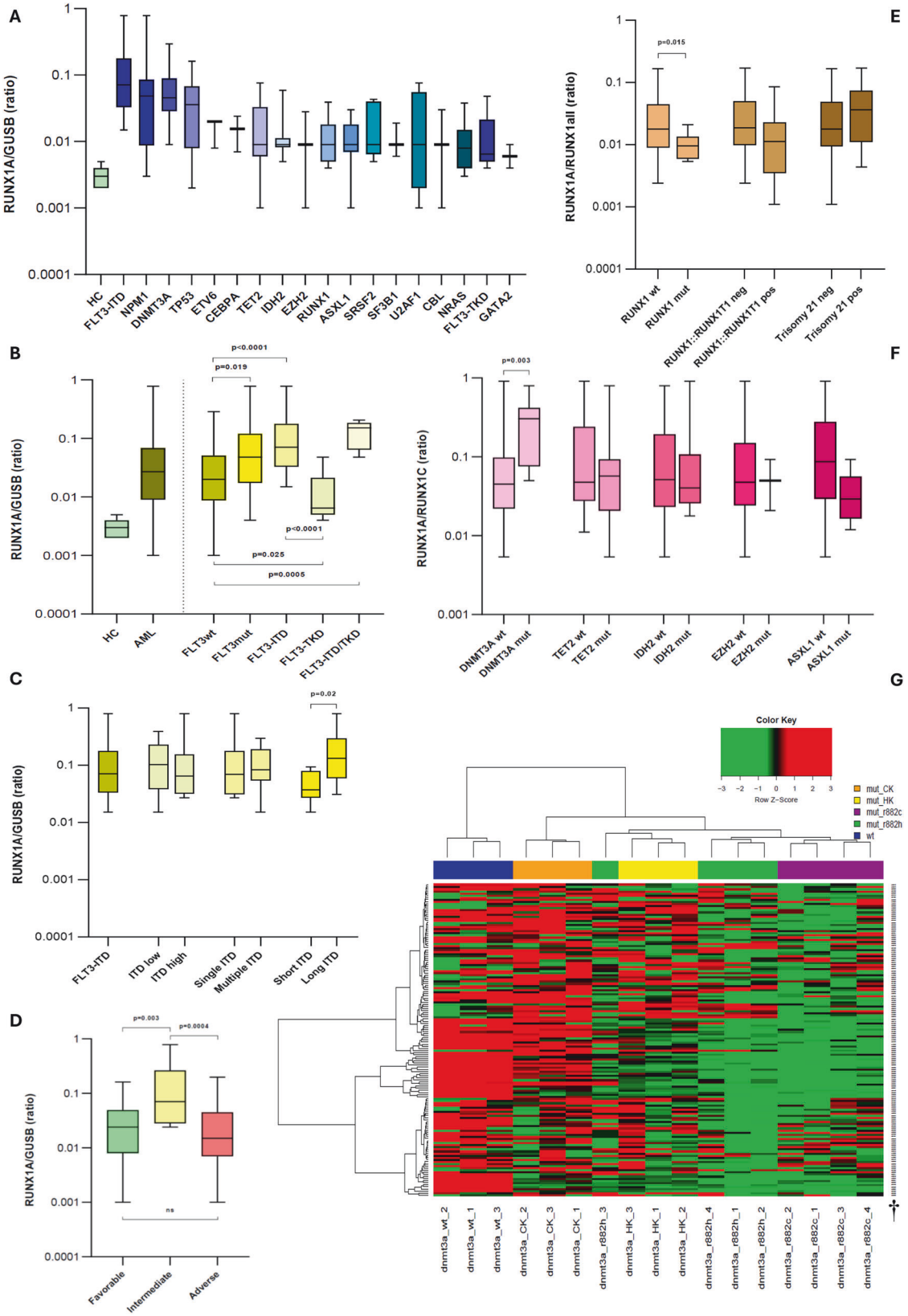

RUNX1A levels than *FLT3*-wt cases, *FLT3*-TKD patients ($n = 10$) had lower *RUNX1A* levels than *FLT3*-wt ones (0.006 vs 0.020 R/G, $p = 0.025$). Again, this observation supports the connection between the ITD mutation and *RUNX1A* expression. Focusing on this aspect, we found that neither the ITD allelic ratio (low vs high) nor the ITD number (single vs multiple) seemed to influence *RUNX1A* transcript levels. However, *RUNX1A* overexpression was higher in long ITD cases ($n = 11$, characterized by more *FLT3* auto-

Fig. 2 Distribution of *RUNX1A* levels in AML. A *RUNX1A* expression according to the patients' mutational profile (from the highest to the lowest *RUNX1A* level). **B** *RUNX1A* transcript level in AML cases subdivided by *FLT3* mutational status; **C** a detailed analysis of *FLT3*-ITD patients is reported. Short ITD: duplication length ≤ 50 bps, long ITD: duplication length > 50 bps. **D** The expression of *RUNX1A* in the AML cases subdivided into the three risk categories according to the ELN 2022 recommendations [33]. **E** *RUNX1A* abundance as a proportion of total *RUNX1* transcripts in patients categorized by main *RUNX1* gene alterations. **F** The *RUNX1A*/*RUNX1C* ratio in AML cases stratified according to the mutational status of key epigenetic modifiers. **G** Hierarchical clustering of methylation values of CpG sites mapping to *RUNX1* based on Illumina methylation annotation in the TF-1 cell line stably expressing wild-type DNMT3A (isoform 1) or AML-associated hotspot mutants (either R882C or R882H) alone or in combination with R676K [27]. CK: R882C/R676K; HK: R882H/R676K. †Probe names.

phosphorylation and poorer survival outcomes [18]) compared to short ITD ones ($n = 8$) (0.131 vs 0.037 R/G, $p = 0.02$) (Fig. 2C). The association between *FLT3*-ITD and *RUNX1A* overexpression indirectly influenced the median levels of the isoform in the three risk categories according to the ELN 2022 recommendations [33]. AML patients in the intermediate category (where all *FLT3*-ITD but not *FLT3*-TKD are included) showed higher *RUNX1A* levels than those in the favorable and adverse categories (0.070 vs 0.024 R/G, $p = 0.003$ and 0.070 vs 0.015 R/G, $p = 0.0004$ respectively), whereas no differences were observed between the latter two categories (Fig. 2D).

Although *RUNX1A* overexpression is strongly associated with *FLT3*-ITD, isoform levels do not appear to influence patients' overall survival (OS) (HR: 0.363, 95% CI: 0.031-4.291, $p = 0.421$) (Supplementary Fig. 3). Finally, the close relationship between *FLT3*-ITD and *RUNX1A* expression was observed again at disease relapse (DR), but this aspect will be discussed later.

DNMT3A-mutated AMLs present higher RUNX1A levels than DNMT3A-wt cases

Although there is a clear association between *RUNX1A* overexpression and the *FLT3*-ITD mutation, we considered other possible genetic mechanisms influencing *RUNX1A* levels in AML, namely *RUNX1* gene alterations (SNVs and INDELs, *RUNX1::RUNX1T1* and trisomy 21), spliceosome mutations (*SRSF2*, *SF3B1*, and *U2AF1* variants) and epigenetic modifiers mutations (*DNMT3A*, *TET2*, *IDH2*, *EZH2*, *ASXL1*).

None of the explored *RUNX1* gene alterations appeared to be associated with isoform A overexpression (absolute levels), including trisomy 21 (as somatic event), unlike what has been described in Down Syndrome—associated myeloid leukemia (ML-DS) [3] (Supplementary Fig. 1A). To better characterize the relationship between isoform A and *RUNX1* gene alterations, we focused also on the *RUNX1A* quantification relative to all *RUNX1* transcripts. Notably, lower *RUNX1A*/*RUNX1*all levels were observed in *RUNX1*-mutated cases ($n = 11$) compared to wild-type ones ($n = 43$)(0.010 vs 0.018, $p = 0.015$), suggesting a mutually exclusive relationship between gene mutations (loss of function and/or altered function [34]) and the expression of the leukemogenic isoform A (Fig. 2E).

Although *RUNX1A* is generated by alternative splicing [35, 36], no differences in *RUNX1A* levels were observed in AML patients carrying spliceosome mutations compared to wild-type cases, neither considering its absolute quantification nor the ratio between the two splicing isoforms *RUNX1A* and *RUNX1B* (Supplementary Figure 1B/C).

Last but not least, we investigated the potential role of mutations in epigenetic modifiers in contributing to the disequilibrium of *RUNX1* isoforms, focusing on the ratio between *RUNX1A* and *RUNX1C*, transcribed from the P2 and P1 promoters, respectively. Interestingly, *DNMT3A*-mutated AML cases ($n = 8$) displayed a significantly higher *RUNX1A*/*RUNX1C* ratio compared to *DNMT3A*–wild-type cases ($n = 46$) (0.304 vs 0.045, $p = 0.0029$), suggesting a possible differential methylation activity of *DNMT3A* on the two promoters (Fig. 2F). This difference remained significant when analyzing *RUNX1A* absolute expression levels (see Supplementary Fig. 1D) so we decided to study the relationship between *DNMT3A* mutational status and the methylation profile of *RUNX1* gene. Recently, TF-1 cell line was engineered to stably expressed *DNMT3A* (isoform 1), including WT and AML-associated hotspot mutants (either R882C or R882H) alone or in combination with R676K, an additional macro-oligomerization-decreasing mutation: R882C/R676K (DNMT3A_CK) and R882H/R676K (DNMT3A_HK) [27]. Comparing their methylation profile, global hypomethylation of *RUNX1* CpG sites was observed in all *DNMT3A*-mutated TF-1 cells compared to *DNMT3A*_WT cells (Fig. 2G). Differential methylation analysis between WT and all *DNMT3A* mutant cell lines revealed statistically significant hypomethylation of almost all CpG sites of *RUNX1*, regardless of the genomic location of the CpG site (data not shown).

RUNX1A overexpression is disease-related and reappears at relapse, with no clear kinetics, except in FLT3-ITD cases

With the aim of studying *RUNX1A* kinetic expression during the disease course, we evaluated the levels at the CR stage and at DR.

When patients achieved CR, their *RUNX1A* levels reverted to normal values (Fig. 3A). In fact, no differences were found between patients at this stage and HC (0.002 vs 0.003, $p = 0.298$) (Fig. 3B).

At DR, we again quantified the expression of all three isoforms. As observed at disease onset, when comparing relapsing AML cases ($n = 21$) with HC we confirmed the overexpression of *RUNX1A* (0.020 vs 0.003 R/G, $p < 0.0001$) and *RUNX1B* (1.167 vs 0.433 R/G, $p = 0.0012$), whereas no difference was observed for *RUNX1C* (0.376 vs 0.322 R/G, $p = 0.341$) (Fig. 3C).

Considering, for each patient, the evolution of *RUNX1* isoforms expression between the diagnosis and DR, no clear kinetics emerged from the analyzed cases (Fig. 3D–G). Notably, when we focused on four cases that were *FLT3*-ITD negative at disease onset but *FLT3*-ITD mutated at DR, all of these cases exhibited an increased *RUNX1A* expression compared to the values at diagnosis ($p = 0.033$), confirming once again the close connection previously demonstrated between *FLT3*-ITD mutations and *RUNX1A* overexpression (Fig. 3H).

Overall, no differences emerged when comparing median *RUNX1A* expression levels between diagnosis and DR (0.027 vs 0.02 R/G, $p = 0.728$), as also when comparing patients in CR with HC (Fig. 3B). In short, *RUNX1A* overexpression was disease-related and this observation holds true not only when considering the median level of isoform A, but also its kinetics in the few cases for which diagnostic, CR and DR samples were available. Three representative examples are shown in Fig. 3I.

RUNX1A overexpression is associated with a specific transcriptional profile

To verify whether *RUNX1A* upregulation is linked to a specific transcriptional profile, high-throughput RNA sequencing was conducted. Interestingly, patients with "high" *RUNX1A* expression (FC ≥ 5) also produced a greater number of *RUNX1A* reads (≥18,000 reads) compared to patients with "normal/low" (FC ≤ 3) *RUNX1A* expression (<12,000 reads), demonstrating a positive correlation of about 90% ($r_s = 0.89$, $p = 0.0002$), indicating the reliability of the sequencing approach. PCA showed the separation between the two groups of samples (high and normal/low *RUNX1A* expression) and highlighted the homogeneity of samples within each group (Fig. 3L).

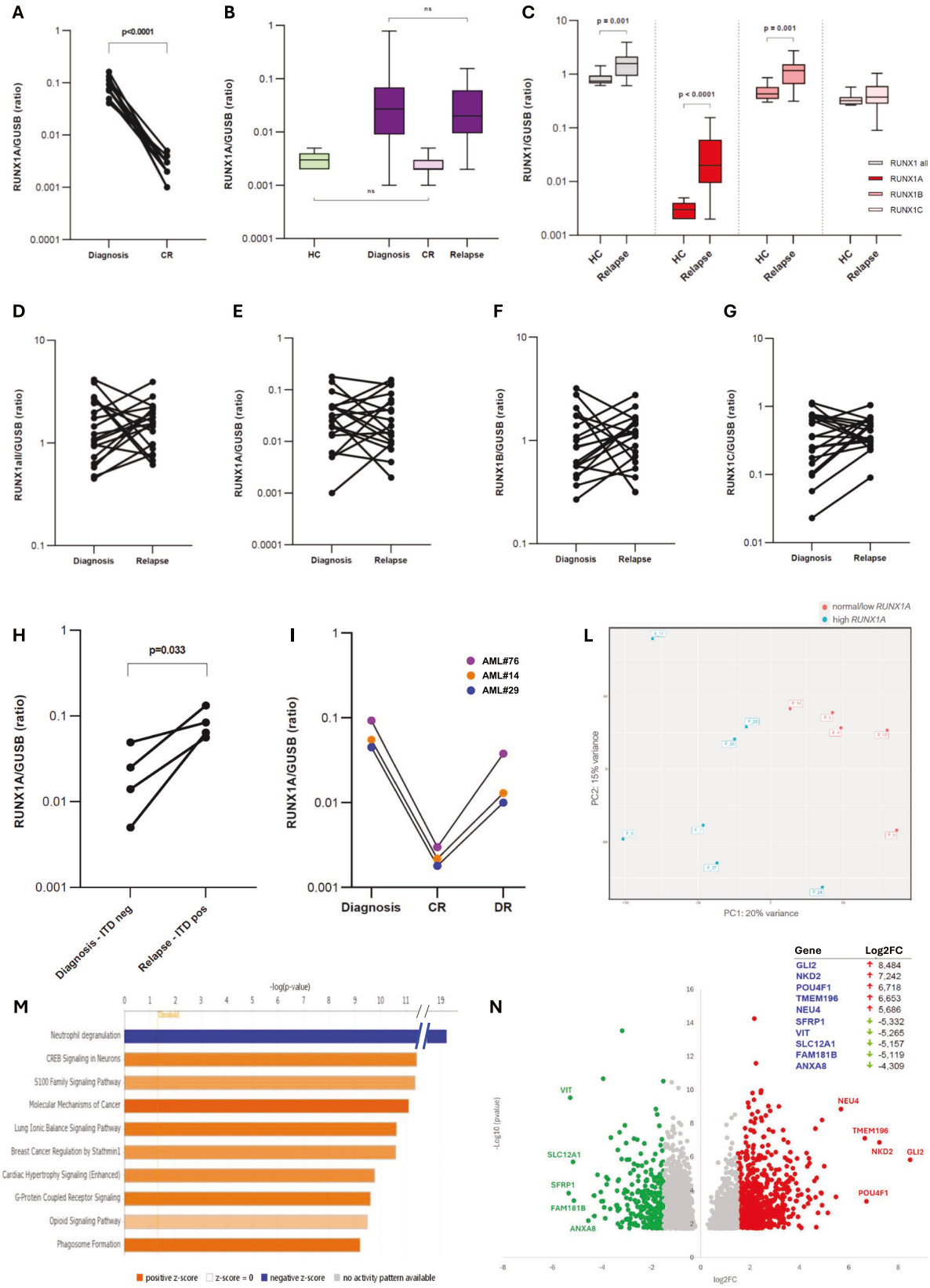

A total of 3622 protein-coding genes (1491 up and 2131 down) and 3108 elements belonging to other categories (lncRNAs, miRNAs, pseudogenes, etc.) were found to be differentially expressed between the two groups of patients. The complete list of differentially expressed elements is reported in Supplementary Table 4. Among these, 756 protein-coding genes (557 up and 199 down) and 1159 elements belonging to other categories (lncRNAs, miRNAs, pseudogenes, etc.) were differentially expressed, with a

Fig. 3 *RUNX1A*, kinetics and RNA-Seq data analysis. A *RUNX1A* kinetics from diagnosis to CR. **B** *RUNX1A* expression during the disease course. **C** Comparison of *RUNX1* expression between healthy controls and AML cases at disease relapse (single isoforms and their sum are reported). **D**–**G***RUNX1* isoforms kinetics from diagnosis to disease relapse for each patient. **H** *RUNX1A* kinetics from diagnosis to disease relapse, for four cases that were *FLT3*-ITD negative at disease onset but *FLT3*-ITD mutated at relapse. **I** Representative examples of *RUNX1A* kinetics (diagnosis, CR, DR) in three patients. **L** Principal Component Analysis (PCA) showing the separation between the two groups of samples (high and normal/low *RUNX1A* expression) and highlighting the homogeneity of samples within each group. **M** Top ten deregulated canonical pathways identified from IPA analysis. **N** Volcano plot visualizing differentially expressed protein-coding genes (with p value < 0.05) between the two groups of patients (high and normal/low *RUNX1A* expression). Upregulated (Log2FC > 1.5) and downregulated (Log2FC < −1.5) genes are marked in red and green, respectively. The top five deregulated protein-coding genes are reported in the table (top–right).

Log2FC > 1.5 or < −1.5 and with a p value and a padj value < 0.05 between the two groups of patients.

Statistically significant (padj < 0.05) DEGs were categorized into Gene Ontology (GO) categories using the online software DAVID (https://david.ncifcrf.gov/tools.jsp). "Signal Transduction" was identified as the TOP BP ($p = 7.00E-07$), "Plasma membrane" the TOP CC ($p = 3.02E-23$), and "serine-type endopeptidase activity" the TOP MF ($p = 2.07E-6$) items. The complete list of gene ontology categories (BP, CC, MF) and the categorized genes are reported in Supplementary Table 5.

Then, a "core analysis" was performed using IPA software, to investigate canonical pathways enriched in DEGs. "Neutrophil degranulation" ($p = 5.85E-20$) was identified as the TOP canonical pathway deregulated, with 56 DEGs; the majority of them being downregulated genes. The activation state of the pathway was identified as "decreased" (z-score = −6682) (Fig. 3M). Interestingly, this observation is in line with the known *RUNX1A* ability to suppress myeloid differentiation [2, 4, 32] and with the higher *RUNX1A* levels observed in our AML cases with a more immature phenotype and characterized by impaired granulocytic differentiation (M0-M3). The complete list of canonical pathways resulting from the analysis is reported in Supplementary Table 6.

Notably, when focusing on the TOP five DEGs (upregulated and downregulated) between the two groups (Fig. 3N), the *POU4F1* (Log2FC = 6.72, padj = 0.009) and *SFRP1* (Log2FC = −5.33, padj=0.005) genes stand out. In fact, *POU4F1* overexpression has already been associated with *RUNX1::RUNX1T1* AML and is known to contribute directly to its unique transcriptional signature; on the contrary, *SFRP1* is a transcriptional repression target of the RUNX1::RUNX1T1 fusion protein in AML [37, 38].

DISCUSSION

The pivotal role of *RUNX1* in the control of hematopoiesis has been amply demonstrated [39]. Dysregulated *RUNX1* can contribute to blood diseases in many ways, whereby either an excess or a deficiency of *RUNX1*, or an altered function, can promote leukemogenesis [34]. Among the main *RUNX1* alterations, gene mutations (germline and somatic) and *RUNX1::RUNX1T1* fusion are the most common events, widely studied in AML pathogenesis [34, 40, 41]. However, additional genetic aberrations (copy number events or further genomic rearrangements) can affect its function [42, 43]. Conversely, less attention has been paid to *RUNX1* expression in AML, even if its overexpression has been associated with poorer outcomes in cytogenetically normal AML [28].

To the best of our knowledge, this is the first study to report the absolute quantification of the three main *RUNX1* isoforms in an AML series. The observed *RUNX1A* and *RUNX1B* overexpression suggests a possible different epigenetic regulation of these two isoforms, transcribed from the P2 promoter (proximal), whereas the expression of *RUNX1C* (transcribed from the P1 promotor—distal) [44, 45] remains unchanged.

Among the three main *RUNX1* isoforms, several studies have shown the leukemogenic role of *RUNX1A* in different hematological diseases. A study on myelodysplastic/myeloproliferative neoplasms (MDS/MPN) showed the involvement of *RUNX1A* in disease progression [7]. A recent study on ML-DS demonstrated the key role of a *RUNX1* isoform disequilibrium favoring *RUNX1A* in the pathogenesis of this rare disease [3]. Even though based on a limited number of cases, *RUNX1A* overexpression was also observed in two previous studies on acute leukemia [2, 6].

In our study, we investigated *RUNX1A* levels in AML and linked its overexpression with key clinical and biological parameters and the disease course. Interestingly, our observations align with the already-known role of *RUNX1* in hematopoiesis. Specifically, the higher levels of *RUNX1A* observed in thrombocytopenic cases confirm the widely demonstrated involvement of the *RUNX1* gene in megakaryocytopoiesis [29]. Furthermore, *RUNX1A* overexpression was recently described in the familial platelet disorder with associated myeloid malignancy (FPDMM), suggesting a new potential role for *RUNX1* isoforms disequilibrium in the development of myeloid malignancy in FPD [8, 9].

The ability of *RUNX1A* to suppress myeloid differentiation while enhancing the HSC self-renewal capacity [2, 4, 32] aligns with the higher *RUNX1A* overexpression observed in the more undifferentiated cases in our cohort. In murine models, enforced expression of *RUNX1A* expanded the immature hematopoietic cell population, conferring the potential to differentiate into multiple lineages ex vivo [4]. Other data showed that overexpressed *RUNX1A* inhibits myeloid cell differentiation and stimulates cell proliferation upon granulocyte colony-stimulating factor (G-CSF) treatment [2].

However, the highest *RUNX1A* levels were observed in *FLT3*-ITD AML patients. The *RUNX1* cooperation with *FLT3*-ITD in leukemia induction is already known [46, 47]. *FLT3*-ITD AML patients express high levels of *RUNX1*; *FLT3*-ITD directly impacts *RUNX1* activity, whereby upregulated and phosphorylated *RUNX1* cooperates with *FLT3*-ITD to induce AML [46, 47]. Notably, no studies have specifically focused on the expression of the three *RUNX1* isoforms. However, Cauchy et al. demonstrated that the *RUNX1* upregulation in FLT3-ITD positive AML may partially result from the presence of an ITD-specific open region of chromatin (a DNase I hypersensitive site - DHS) within the *RUNX1* gene, ~10 kb upstream of exon 6, whose alternative splicing generates the *RUNX1A* isoform (Fig. 4) [46]. Although we cannot verify this direct connection, it is conceivable that in *FLT3*-ITD AML, this open region at the 5′ end of exon 6 may facilitate regulator access, promoting alternative splicing in favor of *RUNX1A* production, as recently described [35]. Moreover, *RUNX1A* overexpression could also result partially from epigenetic mechanisms, as suggested by the higher levels detected in our *DNMT3A*-mutated cases. In fact, as we observed in TF-1 cells, *DNMT3A* dysfunction impacts the *RUNX1* methylation profile.

By studying *RUNX1A* kinetics during follow-up, we highlighted its close association with the disease course. *RUNX1A* overexpression is disease-related and drives a specific transcriptional profile which, in some respects, overlaps the *RUNX1::RUNX1T1* gene expression signature. Notably, *RUNX1A* overexpression is closely linked to *POU4F1* upregulation and *SFRP1* downregulation, two events already observed in *RUNX1::RUNX1T1* AML [37, 38].

The main strength of this study is the strong association observed between *RUNX1A* deregulation and significant AML clinical and biological parameters, particularly the *FLT3*-ITD mutation. However, the hypotheses presented were not verified through functional models (the main limitation of our work); further studies are required to validate these findings.

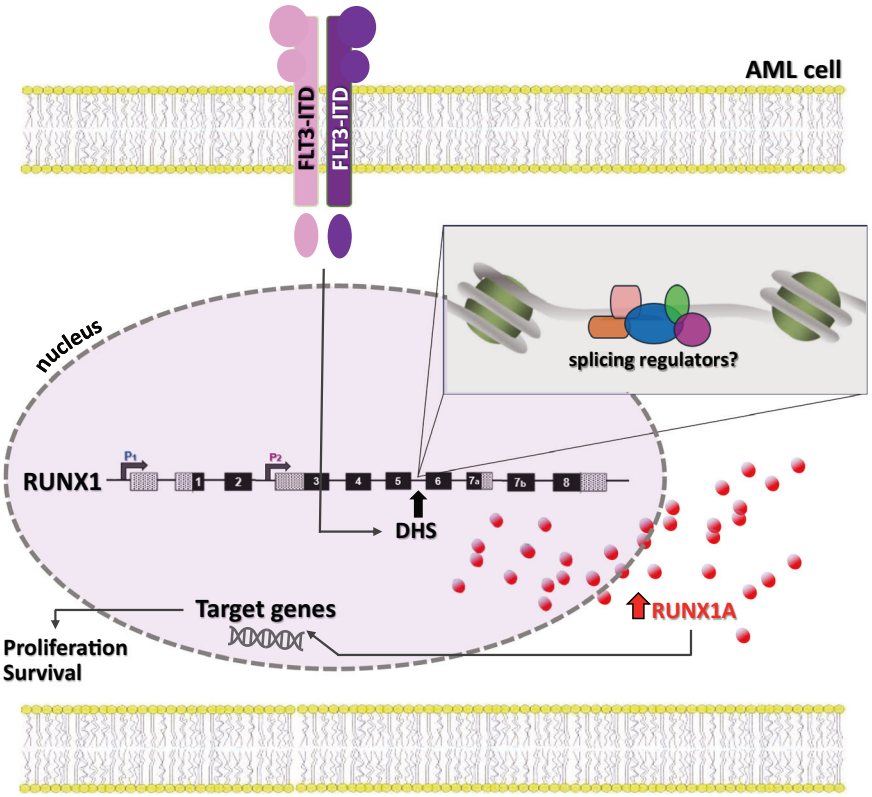

Fig. 4 Illustration of a possible molecular connection between *FLT3*-ITD and *RUNX1A* overexpression, based on recent literature data [35, 46]. CR complete remission, HC healthy controls, AML acute myeloid leukemia, DHS DNase I hypersensitive site.

CONCLUSIONS

The AML biological heterogeneity underscores the need for deeper insights into the molecular mechanisms underlying disease development. Our data aims to contribute a new piece to the jigsaw of the AML molecular pathogenesis, in which *RUNX1* involvement is established. Our effort to shed light on the dark side of *RUNX1* dysregulation may also offer the opportunity to look on *RUNX1A* as a new AML therapeutic target. In fact, restoring the *RUNX1* isoform equilibrium could reverse the oncogenic potential of isoform A, as recently shown in ML-DS. In *FLT3*-ITD AML cases, for which targeted treatments are already available, clarifying unknown aspects of the FLT3 pathway could identify new druggable molecules whose synergistic action with FLT3 inhibitors warrants investigation. In the meantime, another piece has been added to the complex scenario of AML pathogenesis.

DATA AVAILABILITY

The data generated in this study are available upon request from the corresponding author.

REFERENCES

1. Miyoshi H, Ohira M, Shimizu K, Mitani K, Hirai H, Imai T, et al. Alternative splicing and genomic structure of the AML1 gene involved in acute myeloid leukemia. Nucleic Acids Res. 1995;23:2762–9.
2. Tanaka T, Tanaka K, Ogawa S, Kurokawa M, Mitani K, Nishida J, et al. An acute myeloid leukemia gene, AML1, regulates hemopoietic myeloid cell differentiation and transcriptional activation antagonistically by two alternative spliced forms. EMBO J. 1995;14:341–50.
3. Gialesaki S, Bräuer-Hartmann D, Issa H, Bhayadia R, Alejo-Valle O, Verboon L, et al. RUNX1 isoform disequilibrium promotes the development of trisomy 21–associated myeloid leukemia. Blood. 2023;141:1105–18.
4. Tsuzuki S, Seto M. Expansion of functionally defined mouse hematopoietic stem and progenitor cells by a short isoform of RUNX1/AML1. Blood. 2012;119:727–35.
5. Challen GA, Goodell MA. Runx1 isoforms show differential expression patterns during hematopoietic development but have similar functional effects in adult hematopoietic stem cells. Exp Hematol. 2010;38:403–16.
6. Liu X, Zhang Q, Zhang DE, Zhou C, Xing H, Tian Z, et al. Overexpression of an isoform of AML1 in acute leukemia and its potential role in leukemogenesis. Leukemia. 2009;23:739–45.
7. Sakurai H, Harada Y, Ogata Y, Kagiyama Y, Shingai N, Doki N, et al. Overexpression of RUNX1 short isoform has an important role in the development of myelodysplastic/myeloproliferative neoplasms. Blood Adv. 2017;1:1382–6.
8. Engvall M, Karlsson Y, Kuchinskaya E, Jörnegren Å, Mathot L, Pandzic T, et al. Familial platelet disorder due to germline exonic deletions in RUNX1: a diagnostic challenge with distinct alterations of the transcript isoform equilibrium. Leuk Lymphoma. 2022;63:2311–20.
9. Cabrerizo Granados D, Barbosa I, Baliakas P, Hellström-Lindberg E, Lundin V. The clinical phenotype of germline RUNX1 mutations in relation to the accompanying somatic variants and RUNX1 isoform expression. Genes Chromosom Cancer. 2023;62:672–7.
10. Cumbo C, Tarantini F, Anelli L, Zagaria A, Redavid I, Minervini CF, et al. IRF4 expression is low in Philadelphia negative myeloproliferative neoplasms and is associated with a worse prognosis. Exp Hematol Oncol. 2021;10:1–4.
11. Tarantini F, Cumbo C, Parciante E, Anelli L, Zagaria A, Coccaro N et al. IRF4 gene expression on the trail of molecular response: looking at chronic myeloid leukemia from another perspective. Acta Haematol. 2022. https://doi.org/10.1159/000527173.
12. Cumbo C, Tarantini F, Zagaria A, Anelli L, Minervini CF, Coccaro N, et al. Clonal hematopoiesis at the crossroads of inflammatory bowel diseases and hematological malignancies: a biological link?. Front Oncol. 2022;12:1–5.
13. Coccaro N, Zagaria A, Orsini P, Anelli L, Tota G, Casieri P, et al. RARA and RARG gene downregulation associated with EZH2 mutation in acute promyelocytic-like morphology leukemia. Hum Pathol. 2018;80:82–86.
14. Cumbo C, Orsini P, Tarantini F, Anelli L, Zagaria A, Tragni V, et al. TNFRSF13B gene mutation in familial acute myeloid leukemia: a new piece in the complex scenario of hereditary predisposition?. Hematol Oncol. 2023;41:942–6.
15. Murphy KM, Levis M, Hafez MJ, Geiger T, Cooper LC, Smith BD, et al. Detection of FLT3 internal tandem duplication and D835 mutations by a multiplex polymerase chain reaction and capillary electrophoresis assay. J Mol Diagn. 2003;5:96–102.
16. Döhner H, Estey E, Grimwade D, Amadori S, Appelbaum FR, Büchner T et al. *Diagnosis and management of AML in adults: 2017 ELN recommendations from an international expert panel*. 2017 https://doi.org/10.1182/blood-2016-08-733196.

17. Cumbo C, Tarantini F, Anelli L, Zagaria A, Specchia G, Musto P, et al. FLT3 mutational analysis in acute myeloid leukemia: advantages and pitfalls with different approaches. Blood Rev. 2022;54:100928.
18. Polak TB, van Rosmalen J, Dirven S, Herzig JK, Cloos J, Meshinchi S, et al. Association of FLT3-internal tandem duplication length with overall survival in acute myeloid leukemia: a systematic review and meta-analysis. Haematologica. 2022;107:2506–10.
19. Ewels P, Magnusson M, Lundin S, Käller M. MultiQC: summarize analysis results for multiple tools and samples in a single report. Bioinformatics. 2016;32:3047–8.
20. Bolger AM, Lohse M, Usadel B. Trimmomatic: a flexible trimmer for Illumina sequence data. Bioinformatics. 2014;30:2114–20.
21. Dobin A, Davis CA, Schlesinger F, Drenkow J, Zaleski C, Jha S, et al. STAR: ultrafast universal RNA-seq aligner. Bioinformatics. 2013;29:15–21.
22. Liao Y, Smyth GK, Shi W. FeatureCounts: an efficient general purpose program for assigning sequence reads to genomic features. Bioinformatics. 2014;30:923–30.
23. Love MI, Huber W, Anders S. Moderated estimation of fold change and dispersion for RNA-seq data with DESeq2. Genome Biol. 2014;15:1–21.
24. Sherman BT, Hao M, Qiu J, Jiao X, Baseler MW, Lane HC, et al. DAVID: a web server for functional enrichment analysis and functional annotation of gene lists (2021 update). Nucleic Acids Res. 2022;50:W216–W221.
25. Huang DW, Sherman BT, Lempicki RA. Systematic and integrative analysis of large gene lists using DAVID bioinformatics resources. Nat Protoc. 2009;4:44–57.
26. Krämer A, Green J, Pollard J, Tugendreich S. Causal analysis approaches in ingenuity pathway analysis. Bioinformatics. 2014;30:523–30.
27. Lu J, Guo Y, Yin J, Chen J, Wang Y, Wang GG, et al. Structure-guided functional suppression of AML-associated DNMT3A hotspot mutations. Nat Commun. 2024;15:1–16.
28. Fu L, Fu H, Tian L, Xu K, Hu K, Wang J, et al. High expression of RUNX1 is associated with poorer outcomes in cytogenetically normal acute myeloid leukemia. Oncotarget. 2016;7:15828–39.
29. Wang C, Tu Z, Cai X, Wang W, Davis AK, Nattamai K, et al. A critical role of RUNX1 in governing megakaryocyte-primed hematopoietic stem cell differentiation. Blood Adv. 2023;7:2590–605.
30. Khoury JD, Solary E, Abla O, Akkari Y, Alaggio R, Apperley JF, et al. The 5th edition of the World Health Organization Classification of Haematolymphoid Tumours: myeloid and histiocytic/dendritic neoplasms. Leukemia. 2022;36:1703–19.
31. Bennett JM, Catovsky D, Daniel M-T, Flandrin G, Galton DAG, Gralnick HR, et al. Proposals for the Classification of the Acute Leukaemias French-American-British (FAB) Co-operative Group. Br J Haematol. 1976;33:451–8.
32. Tsuzuki S, Hong D, Gupta R, Matsuo K, Seto M, Enver T. Isoform-specific potentiation of stem and progenitor cell engraftment by AML1/RUNX1. PLoS Med. 2007;4:0880–96.
33. Döhner H, Wei AH, Appelbaum FR, Craddock C, DiNardo CD, Dombret H, et al. Diagnosis and management of AML in adults: 2022 recommendations from an international expert panel on behalf of the ELN. Blood. 2022;140:1345–77.
34. Kellaway SG, Coleman DJL, Cockerill PN, Raghavan M, Bonifer C. Molecular basis of hematological disease caused by inherited or acquired RUNX1 mutations. Exp Hematol. 2022;111:1–12.
35. Davis AG, Einstein JM, Zheng D, Jayne ND, Fu XD, Tian B, et al. A CRISPR RNA-binding protein screen reveals regulators of RUNX1 isoform generation. Blood Adv. 2021;5:1310–23.
36. Komeno Y, Yan M, Matsuura S, Lam K, Lo MC, Huang YJ, et al. Runx1 exon 6-related alternative splicing isoforms differentially regulate hematopoiesis in mice. Blood. 2014;123:3760–9.
37. Fortier JM, Payton JE, Cahan P, Ley TJ, Walter MJ, Graubert TA. POU4F1 is associated with t(8;21) acute myeloid leukemia and contributes directly to its unique transcriptional signature. Leukemia. 2010;24:950–7.
38. Cheng CK, Li L, Cheng SH, Ng K, Chan NPH, Ip RKL, et al. Secreted-frizzled related protein 1 is a transcriptional repression target of the t(8;21) fusion protein in acute myeloid leukemia. Blood. 2011;118:6638–48.
39. De Bruijn M, Dzierzak E. Runx transcription factors in the development and function of the definitive hematopoietic system. Blood. 2017;129:2061–9.
40. Bellissimo DC, Speck NA. RUNX1 mutations in inherited and sporadic leukemia. Front Cell Dev Biol. 2017;5:1–11.
41. Sood R, Kamikubo Y, Liu P. Role of RUNX1 in hematological malignancies. Blood. 2017;129:2070–82.
42. Cumbo C, Tota G, De Grassi A, Anelli L, Zagaria A, Coccaro N, et al. RUNX1 gene alterations characterized by allelic preference in adult acute myeloid leukemia. Leuk Lymphoma. 2021;0:1–9.
43. Zagaria A, Anelli L, Coccaro N, Tota G, Casieri P, Cellamare A, et al. 5′RUNX1-3′ USP42 chimeric gene in acute myeloid leukemia can occur through an insertion mechanism rather than translocation and may be mediated by genomic segmental duplications. Mol Cytogenet. 2014;7:1–8.
44. Levanon D, Glusman G, Bangsow T, Ben-Asher E, Male DA, Avidan N, et al. Architecture and anatomy of the genomic locus encoding the human leukemia-associated transcription factor RUNX1/AML1. Gene. 2001;262:23–33.
45. Ghozi MC, Bernstein Y, Negreanu V, Levanon D, Groner Y. Expression of the human acute myeloid leukemia gene AML1 is regulated by two promoter regions. Proc Natl Acad Sci USA. 1996;93:1935–40.
46. Cauchy P, James SR, Zacarias-Cabeza J, Ptasinska A, Imperato MR, Assi SA, et al. Chronic FLT3-ITD signaling in acute myeloid leukemia is connected to a specific chromatin signature. Cell Rep. 2015;12:821–36.
47. Behrens K, Maul K, Tekin N, Kriebitzsch N, Indenbirken D, Prassolov V, et al. RUNX1 cooperates with FLT3-ITD to induce leukemia. J Exp Med. 2017;214:737–52.

ACKNOWLEDGEMENTS

This work was supported by "Associazione Italiana contro le Leucemie (AIL)-BARI".

AUTHOR CONTRIBUTIONS

Conception and design of the study: CC and FA. Acquisition of data and/or analysis and interpretation of data: CC, FT, EP, LA, AZ, NC, GT, IR, MRC, AM, CFM, GS, PM, and FA. Clinical data acquisition: FT, VPG, and MD. Protein quantification: GB, AN, and FG. RNA-sequencing: MFC, FM, CT, SNC, BB and AT. Methylation analysis: PO and MG. Drafting of the manuscript: FA. All authors revised the manuscript for important intellectual content and approved the final version submitted for publication.

FUNDING

Open access funding provided by Università degli Studi di Roma Tor Vergata within the CRUI-CARE Agreement.

COMPETING INTERESTS

The authors declare no competing interests.

ETHICS APPROVAL AND CONSENT TO PARTICIPATE

The local Ethics Committee of "Azienda Ospedaliero Universitaria Policlinico di Bari" approved the study. Informed consent was obtained from all patients before study inclusion, in accordance with the Declaration of Helsinki. Patients' records/information were anonymized and de-identified before analysis.

ADDITIONAL INFORMATION

Supplementary information The online version contains supplementary material available at https://doi.org/10.1038/s41417-025-00939-z.

Correspondence and requests for materials should be addressed to Francesco Albano.